

Micro-scale fluid and odorant transport to antennules of the crayfish, *Procambarus clarkii*

Swapnil Pravin · DeForest Mellon Jr. ·
Matthew A. Reidenbach

Received: 22 November 2011 / Revised: 13 May 2012 / Accepted: 16 May 2012 / Published online: 5 June 2012
© Springer-Verlag 2012

Abstract A numerical model was developed to determine advective–diffusive transport of odorant molecules to olfactory appendages of the crayfish, *Procambarus clarkii*. We tested the extent of molecule transport to the surfaces of aesthetasc sensilla during an antennule flick and the degree of odorant exchange during subsequent flicks. During the rapid downstroke of a flick, odorant molecules are advected between adjacent aesthetascs, while during the slower return stroke, these odorants are trapped between the sensilla and molecular diffusion occurs over a sufficient time period to transport odorants to aesthetasc surfaces. During subsequent flicks, up to 97.6 % of these odorants are replaced with new odorant molecules. The concentration of molecules captured along aesthetasc surfaces was found to increase with increased gap spacing between aesthetascs, flick speed, and distance from the proximal end of the aesthetasc, but these changes in morphology and flicking kinematics reduce the animal’s ability to take discrete samples of the odorant-laden fluid environment with each flick. Results suggest that antennule flicking allows discrete sampling of the time- and space-varying odorant signal, and high concentration odorant filaments can be distinguished from more diffuse, low

concentration filaments through changes in both the timing and the encounter rate of odorant molecules to aesthetasc surfaces.

Keywords Chemosensing · Crayfish · Olfaction · Aesthetasc · Diffusion

Introduction

Chemosensing in aquatic crustaceans is a commonly observed phenomenon that enables these animals to locate food, habitat, and prey (Atema 1996; Grasso and Basil 2002; Moore and Crimaldi 2004) and engage in intraspecific communication (Horner et al. 2008). Aquatic crustaceans have microscopic sensory organs, called aesthetascs, arrayed on their antennules that serve as organs of chemosensing. The antennules of decapod crustaceans such as lobsters, crabs and crayfish have two branches, called flagella, and the lateral flagellum of an antennule bears the arrays of olfactory aesthetasc sensilla. While a variety of chemosensory sensilla found on antennules, as well as on other appendages, are involved in various aspects of food-odor tracking (Keller et al. 2003), the aesthetascs alone appear to be involved in processing odorants from conspecifics (Johnson and Atema 2005; Horner et al. 2008). Although a great diversity of antennule morphologies are found across various aquatic species (Beltz et al. 2003; Ache and Young 2005; Koehl 2006; Webster and Weissburg 2009), the mechanism behind odorant sensing in most of these organisms is a periodic flicking of their lateral flagellum against the flow. This results in advection and subsequent entrapment of odorant molecules adjacent to arrays of aesthetasc hairs (Stacey et al. 2002; Koehl 2006; Reidenbach et al. 2008; Schuech et al. 2012). Small-scale

S. Pravin (✉)
Department of Mechanical and Aerospace Engineering,
University of Virginia, Charlottesville, VA 22904, USA
e-mail: sp8yh@virginia.edu

D. Mellon Jr.
Department of Biology, University of Virginia,
Charlottesville, VA 22904, USA

M. A. Reidenbach
Department of Environmental Sciences, University of Virginia,
Charlottesville, VA 22904, USA

advection and molecular diffusion transport these molecules to the surface of the aesthetascs where odorants can be detected by the chemoreceptor neurons (Atema 1995; Koehl 2006).

Within aquatic environments, the distribution of odorants in both space and time is complex, and odorant plumes are often composed of filaments of chemicals at high concentrations adjacent to fluid with little or no odorant (Webster and Weissburg 2001; Crimaldi and Koseff 2001; Atema 1995; Reidenbach and Koehl 2011). This filamentous odor structure varies with distance from the odorant source and depends on factors such as the scales of turbulence in the water flow, and the topography over which the fluid is moving (Moore and Grills 1999; Webster and Weissburg 2009). Flicking in crustaceans has been shown to increase the fluid transport and the flux of odorants to aesthetasc surfaces (Koehl 2006; Stacey et al. 2002). This flicking is analogous to taking a ‘sniff’ of odor (Koehl et al. 2001). Although other studies have quantified the importance of antennule flicking on the ‘leakiness’ of air or water surrounding aesthetascs, few have quantified how this behavior impacts the advective–diffusive transport of odorants to aesthetasc surfaces. Quantifying advective–diffusive transport of dissolved odorants in fluids is a much more complicated analysis and ultimately is more important in determining actual odorant detection. In addition, although trapping of fluid between adjacent aesthetascs has been studied in detail, discrete sampling of odorants has not.

The first step in the process of smelling is the interception of odorants in the surrounding water by olfactory organs. The relative importance of viscous to inertial forces in determining flow around a biological structure, such as an antennule or aesthetasc, is defined by the Reynolds number, $Re = \rho UL/\mu$, where ρ is the density, μ the dynamic viscosity, U the velocity and L is the characteristic length scale of the biological structure (e.g. antennule or aesthetasc diameter). While the inertial forces for the flow at the length scale of an antennule during a flick cannot be ignored (such as turbulent mixing of odorant molecules in the antennule wake), the viscous forces at the length scale of an aesthetasc are much more dominant than inertial forces and the flow behavior is largely laminar. Reynolds number for sensillar hairs of various arthropods ranges from 10^{-4} to 10 (Koehl 2011). Such a flow facilitates the development of a layer of slow moving fluid around the surface of the aesthetascs, called the boundary layer. The boundary layer is relatively thick for low Re , meaning that molecular diffusion is the primary mode of transport of odorant molecules adjacent to the surfaces of aesthetascs.

Previous studies have shown that the time course of molecular diffusion of odorants to the chemoreceptors has a significant bearing on neural responses (Getchell and Getchell 1977; DeSimone 1981; Nachbar and Morton

1981; Moore et al. 1989), while others have argued that molecular diffusion does not play a limiting role in access of odorant molecules to chemoreceptors (Boeckh et al. 1965; Futrelle 1984; Mankin and Mayer 1984). These hypotheses have been tested using calculations of odorant molecule flux to the aesthetasc surface based on assumptions regarding the near aesthetasc flow field (Adam and Delbrück 1968; Berg and Purcell 1977; Murray 1977; Schuech et al. 2012) or measurements of flow velocities surrounding aesthetascs utilizing particle-image velocimetry on dynamically scaled models (Stacey et al. 2002; Reidenbach et al. 2008). However, due to the exceedingly small scales at which transport occurs, $O(\mu\text{m})$, direct observations or measurements of odorant transport to aesthetasc surfaces have proven difficult.

Despite our knowledge that flicking in crustaceans enhances response to odorants (Schmitt and Ache 1979), the flow structure created by a flicking antennule and its impact on chemical transport to aesthetasc surfaces remains poorly understood. Therefore, numerical models are useful tools in understanding the impact of organism morphology and flow kinematics on chemosensing at these relatively small scales. The objective of this study is to determine the impact of antennule morphology and flicking kinematics on odorant molecule capture along aesthetasc surfaces. This study presents a numerical model of flow and odorant transport to the surfaces of aesthetascs along the lateral antennule of the freshwater crayfish, *Procambarus clarkii*. The aesthetascs on the antennules of *P. clarkii* usually occur in pairs on each lateral flagellar annulus, and this relatively simple geometry, combined with an understanding of the large-scale flow around the antennular flagellum (Humphrey and Mellon 2007), enables us to calculate the time-course of odorant delivery to aesthetasc surfaces during a flick. The specific questions we address using this numerical model are:

1. What effect does the gap width between adjacent aesthetascs have on the concentration of molecules transported to the aesthetasc surface?
2. What effect does the velocity of the antennular flick have on the concentration of molecules transported to the aesthetasc surface?
3. Do odorant filaments of different thickness affect the concentration of molecules transported to the aesthetasc surface?
4. Does the location along the aesthetasc surface impact the concentration of molecules transported to its surface?

Methods

The antennular flagella of *P. clarkii* contain arrays of aesthetascs that usually occur in pairs (but sometimes in an



Fig. 1 **a** Antennular flagellum of *Procambarus clarkii*. Grid in background is 1 cm by 1 cm. **b** Annuli of an antennule of *P. clarkii*. Aesthetasc sensilla (shown by black arrows) are arrayed ventrally on each annulus of the distal half of the flagellum

array of up to four aesthetascs), and are located distally on the ventral surface of the lateral antennular flagellum (Fig. 1). These aesthetascs are small hair-like structures that contain about 170 olfactory receptor neurons (ORN) and have a thin cuticle that is permeable to odorant molecules (Mellon et al. 1989). The ORN connect to the ipsilateral olfactory lobe of the brain and encode information provided by chemoreceptor proteins targeted to specific olfactory determinants (Mellon and Humphrey 2007). Each aesthetasc is approximately 100 μm in length, 15–20 μm in base diameter, and less than 10 μm in tip diameter (Mellon et al. 1989). There is a ~1.9-μm thick cuticle that shows a notable change to transparency approximately three-fifths of the way from base to tip, where the majority of chemosensory cells are located (Mellon et al. 1989). The paired aesthetascs are spaced approximately one sensillum diameter apart. The flicking motion of the antennule is mediated by a single muscle, leading to a fast downstroke and a relatively slower return stroke (Mellon 1997). Video recordings of adult *P. clarkii* indicate that antennule flicks occur over a 2 mm distance at average speeds of 1.8 and 1.1 cm s⁻¹ for the downstroke and return stroke, respectively. The average flicking rate of crayfish was measured to be 3.3 flicks s⁻¹ but varies considerably depending upon environmental conditions (Mellon 1997), and flicks occur irregularly and infrequently when stimuli are lacking.

To determine how flicking and antennule morphology impact odorant transport to chemosensory sensilla, we constructed a 2D rectangular flow domain perpendicular to the antennule in which the fluid along with odorant enters and diffuses to the surface of the aesthetascs (Fig. 2). The forward and return motions of the flicking antennule were numerically modeled by making the boundary condition a function of time which corresponds to the speed of a typical flick. The aesthetasc sensilla are oriented at 45° to the antennules and we have used a circular shape to represent

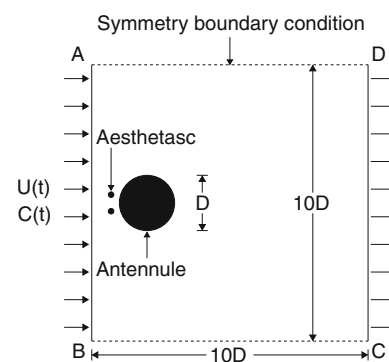


Fig. 2 Schematics of flow past the antennule and aesthetascs

the cross section of the aesthetascs lying within the 2D flow domain. The governing equations for this flow model are:

$$\frac{\partial u}{\partial x} + \frac{\partial v}{\partial y} = 0 \tag{1}$$

$$\frac{\partial u}{\partial t} + u \frac{\partial u}{\partial x} + v \frac{\partial u}{\partial y} = -\frac{1}{\rho} \frac{\partial p}{\partial x} + \nu \left(\frac{\partial^2 u}{\partial x^2} + \frac{\partial^2 u}{\partial y^2} \right) \tag{2}$$

$$\frac{\partial v}{\partial t} + u \frac{\partial v}{\partial x} + v \frac{\partial v}{\partial y} = -\frac{1}{\rho} \frac{\partial p}{\partial y} + \nu \left(\frac{\partial^2 v}{\partial x^2} + \frac{\partial^2 v}{\partial y^2} \right) \tag{3}$$

where u and v are velocity components along x and y axes, respectively, ρ is the density, ν is the kinematic viscosity and p is the pressure. Equation (1) is the continuity equation for a 2D incompressible flow and Eqs. (2) and (3) represent momentum transport along x and y directions, respectively. The velocity components obtained from these equations are used to calculate the odorant concentration from the convective–diffusive equation for scalar transport which is given by:

$$\frac{\partial C}{\partial t} + u \frac{\partial C}{\partial x} + v \frac{\partial C}{\partial y} = D \left(\frac{\partial^2 C}{\partial x^2} + \frac{\partial^2 C}{\partial y^2} \right) \tag{4}$$

where D is the coefficient of diffusivity of the odorant in water. Typically, odorants that attract crustaceans are

composed of amino acids with a molecular diffusivity of $D = 10^{-9} \text{ m}^2 \text{ s}^{-1}$ (Lide 1991).

The boundary conditions for the flow domain (Fig. 2) are:

- **Inlet boundary AB:** The fluid is assumed to enter the inlet boundary with the inlet velocity being a parabolic function of time, to represent water motion relative to a flicking antennule. The antennule within the frame of reference is stationary and the boundary conditions therefore create the moving reference frame relative to the antennule. The water and odorant flow at the inlet are described by:

$$U(t) = \begin{cases} -4U_{pf} \frac{t(t-t_1)}{t_1^2} & \text{if } 0 < t < t_1 \\ -4U_{pr} \frac{(t-t_1)(t-t_2)}{(t_2-t_1)^2} & \text{if } t_1 < t < t_2 \end{cases} \quad (5)$$

$$C(t) = \begin{cases} -4C_\infty \frac{t(t-t_1)}{t_1^2} & \text{if } 0 < t < t_1 \\ -4C_\infty \frac{(t-t_1)(t-t_2)}{(t_2-t_1)^2} & \text{if } t_1 < t < t_2 \end{cases} \quad (6)$$

where U_{pf} and U_{pr} are, respectively, the peak velocities for forward and return strokes of a flick, C_∞ is the ambient concentration of odorant molecules, t_1 is the time duration of the downstroke and t_2 is the time duration of the entire forward and return motion. These boundary conditions are depicted in Fig. 3, where we have assumed a parabolic profile for both the forward and the return strokes, which were approximated from motion analysis of crayfish flicking. The initial conditions assume that the crayfish begins the flick when there is an odorant-containing filament a distance 0.25 mm in front of the antennule, with a filament width thicker than a flick span, and a concentration of $C_\infty = 10^{-8} \text{ kg m}^{-3}$.

- **Outlet boundary CD:** An ‘open’ boundary condition is used for velocity at the outlet boundary. Such a boundary condition allows the fluid to cross the boundary surface in either direction and allows for the model to conserve continuity (Eq. 1). The pressure

is specified as $p_{\text{opening}} = p_{\text{specified}}$, where $p_{\text{specified}} = 0$. This pressure is interpreted as relative total pressure for inflow and relative static pressure for outflow. For flow into the domain, the value of the concentration variable at the opening boundary is specified as $C_{\text{opening}} = C_{\text{specified}}$. For flow out of the domain, no specified value is mandated.

- **The top and bottom boundaries AD and BC:** Symmetry boundary conditions are used for these boundaries, which impose constraints that mirror the flow on either side of it. The velocity component normal to the symmetry plane boundary is set to zero: $U_n = 0$ and the concentration gradient normal to the boundary is also set to zero: $\partial C / \partial n = 0$.
- **Antennule and aesthetasc walls:** The boundary condition at the walls of the antennule and aesthetascs is the no-slip condition for velocity ($U_n = 0$) and zero flux condition for concentration ($-D\nabla C = 0$).

The flow domain was meshed into triangular and quadrilateral cells using the commercially available CFX® Mesh tool. A denser mesh with inflated boundaries was created around the antennule and both aesthetascs to achieve a finer resolution in those regions. Figure 4 shows a zoomed-in view of a high concentration of mesh grid cells close to the aesthetasc surface. Grid cells with characteristic size of $\sim 0.15 \mu\text{m}$ are created around the aesthetasc surface while cells of size $\sim 5 \mu\text{m}$ are created around the antennule surface. A high-resolution transient CFX® solver is used to obtain fluid velocity and concentration values throughout the domain for the duration of a flick and return sequence. We have assumed that odorant molecules can be detected by neurons lining the aesthetasc surface if they are located at a distance of $0.15 \mu\text{m}$ or less from the surface, i.e., within the grid adjacent to the aesthetasc surface. To be detected by neurons lining the aesthetasc surface, odorant molecules must first diffuse across the porous cuticle, whose thickness has been measured for

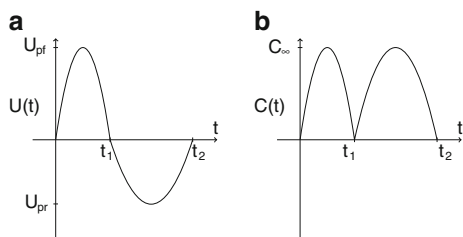


Fig. 3 **a** Velocity and **b** odorant concentration at inlet boundary. Both the quantities are assumed to have a parabolic time-dependent influx to represent the flicking motion of the antennule. $t_1 = 0.118 \text{ s}$ represents the end of downstroke and $t_2 = 0.297 \text{ s}$ represents the end of the entire forward–return sequence, as measured from video recordings of antennule flicking by adult *P. clarkii*

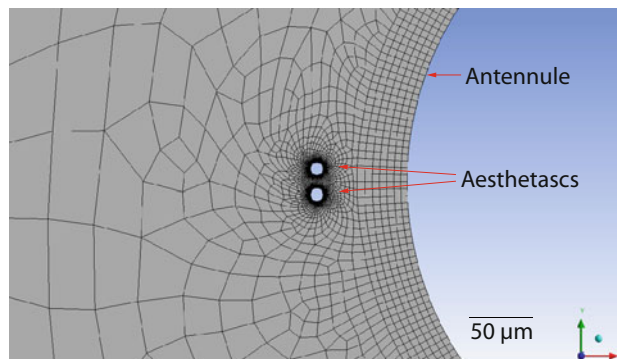


Fig. 4 Mesh grid cells around the aesthetascs and antennule. Cell size adjacent to the aesthetasc surface is $\sim 0.15 \mu\text{m}$ and that around the antennule surface is $\sim 5 \mu\text{m}$

P. clarkii as 1.9 μm (Mellon et al. 1989). Assuming the diffusivity of odorant molecules through the cuticle is similar to that of odorant molecules in water, the timescale for diffusion can be computed as $t = x_{\text{rms}}^2/2D = 2.1 \text{ ms}$ (Denny 1993), where x_{rms} is the root mean squared distance of odorant diffusion. Hence, the assumption is that the odorant molecules present in the grid cell adjacent to the aesthetasc surface will diffuse quickly across the cuticle to chemosensory neurons and can serve as a proxy for odorant concentration that is detected. The average concentration of odorants on the aesthetasc surface over the duration of a flick, C_{mean} , is calculated from the average of grid cells located adjacent to the aesthetasc surface. In addition, four points, evenly distributed around each of the aesthetascs, are examined to provide insight into the distribution of odorant concentrations at different locations along the aesthetasc surface.

Results

Concentration contours (normalized by C_{∞}) at the end of downstroke and return stroke are shown in Fig. 5 for both the entire domain (Fig. 5a, b) and the zoomed-in domain surrounding the aesthetascs (Fig. 5c, d). The concentration contour at the end of the flick (Fig. 5e) shows a significant amount of odorant surrounding the aesthetascs after the flick has finished and hence provides evidence for entrapment of odorant molecules between the aesthetasc pair. Locations on the aesthetasc surface corresponding to $\theta = 180^\circ$ (location on the aesthetasc that faces the ambient flow) and $\theta = 270^\circ$ (location on the aesthetasc that faces the paired aesthetasc) receive the highest concentration of odorants, followed by locations at $\theta = 90^\circ$ and $\theta = 0^\circ$,

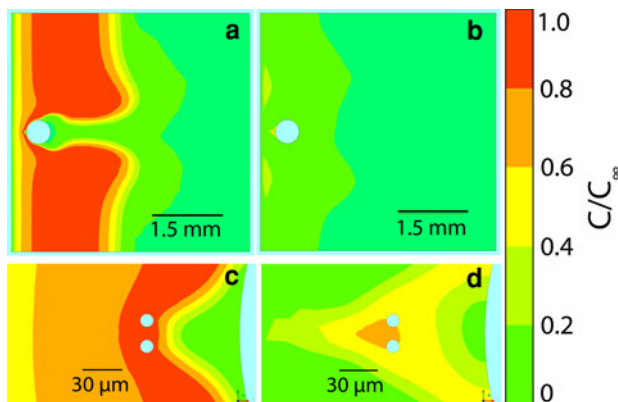


Fig. 5 Concentration contours (normalized by C_{∞}) at the end of **a** downstroke and **b** return stroke, and zoomed in images of concentration surrounding the aesthetascs at the end of the **c** downstroke and **d** return stroke. A region of trapped odorant molecules between the aesthetascs can be seen at the end of return stroke

respectively (Fig. 6). Overall, the rate of change of odorant concentration with time is greatest at the front edge of the aesthetasc and along the surface facing away from the paired aesthetasc (Fig. 7).

The flushing of previously captured odorant and its replacement with new odorant molecules during successive flicks is vital to allow for discrete sampling of odorant distributions within a crustacean’s surroundings. To test the relative magnitude of the exchange of odorant molecules to aesthetasc surfaces between successive flicks, a set of simulations was conducted where the initial condition for

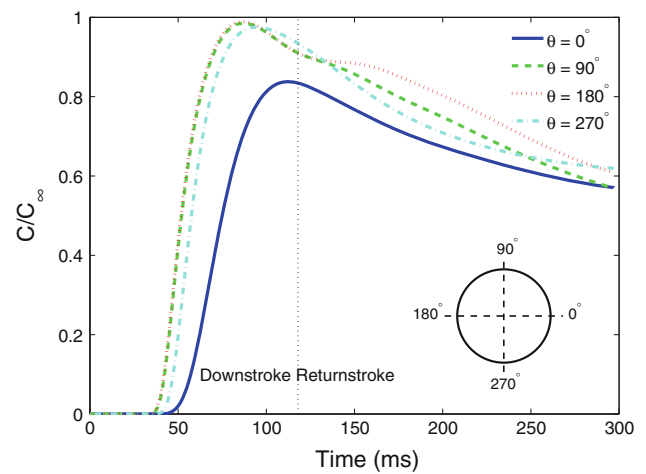


Fig. 6 Normalized odorant concentration at four different locations on the surface of an aesthetasc during a downstroke/return stroke flick sequence. For this aesthetasc geometry, $\theta = 180^\circ$ represents the location on the aesthetasc that faces the ambient flow, while $\theta = 270^\circ$ represents the location on the aesthetasc that faces the other aesthetasc

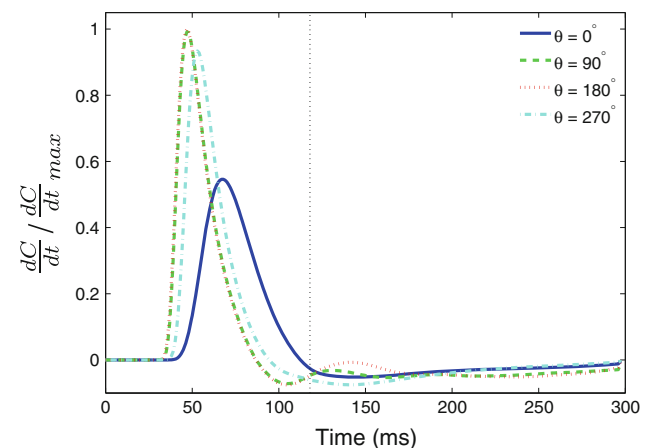


Fig. 7 Rate of normalized concentration change at four different locations on the surface of an aesthetasc during a downstroke/return stroke flick sequence. For this aesthetasc geometry, $\theta = 180^\circ$ represents the location on the aesthetasc that faces the ambient flow, while $\theta = 270^\circ$ represents the location on the aesthetasc that faces the other aesthetasc

odorant molecules concentrations within the flow domain was taken to be the concentration of trapped molecules between the aesthetascs resulting from the previous flick (as shown in Fig. 5d). Two types of inlet boundary conditions were prescribed: (1) the antennule flicking into an odorant filament of concentration C_∞ or (2) the antennule flicking into fresh water ($C = 0 \text{ kg m}^{-3}$). Figure 8 shows the concentration levels for both cases. The total concentration levels observed in Fig. 8 give the combined value of both new and old odorant concentrations, while the line labeled ‘old’ gives the concentration of old molecules only. The subtraction of the two lines gives the concentration of new molecules captured during a successive flick. The line labeled ‘new’ indicates that 97.6 % of odorants along the surface of the aesthetasc have been replaced by new

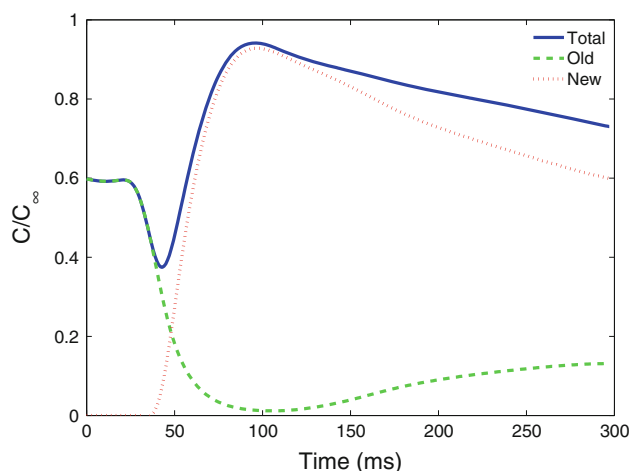


Fig. 8 Concentration at aesthetasc surface for a second flick following an initial flick. Components of total odorant concentration are new odorant molecules acquired in the second flick and the old molecules remaining from the initial flick

molecules by the end of the downward flick. During the return stroke, flow reversal leads to some mixing of new molecules with residual old molecules from the previous flick in the wake of the antennule. This causes an increase in the proportion of old molecules sampled, but the new molecules still constitute 78.1 % of total molecules sampled on the aesthetasc surface at the end of the return stroke. These results provide evidence that: (1) the old molecules are effectively flushed out and (2) new odorant molecules are captured along the aesthetasc surface during a subsequent flick.

To determine the impact of different odorant filament thicknesses on molecule capture, we examined the case when the organism encounters filaments of varying widths, either at the start or near the end of its downstroke. An antennule flicking into a thin odorant filament spends a part of its flick time outside the odorant-laden region. A schematic representing such a situation is shown in Fig. 9. The boundary condition for a filament placed at the beginning of a flick is given by:

$$C(t) = \begin{cases} -4C_\infty \frac{t(t-t_1)}{t_1^2} & \text{if } 0 < t < T_1 \\ 0 & \text{if } T_1 < t < T_2 \\ -4C_\infty \frac{(t-t_1)(t-t_2)}{(t_2-t_1)^2} & \text{if } T_2 < t < t_2 \end{cases} \quad (7)$$

where T_1 is the time when the antennule exits the odorant filament during the downstroke and T_2 is the time when it reenters the odorant filament region during the return stroke. Boundary conditions for velocity and concentration are shown in Fig. 10 for an odorant filament encountered at the beginning of the downstroke. A similar boundary condition is employed for the filaments encountered at the end of a downstroke. The filament sizes tested were varied by the values of T_1 and T_2 given in Tables 1 and 2 for filaments encountered at start and end of a downstroke, respectively. For both encounters with filaments at the start

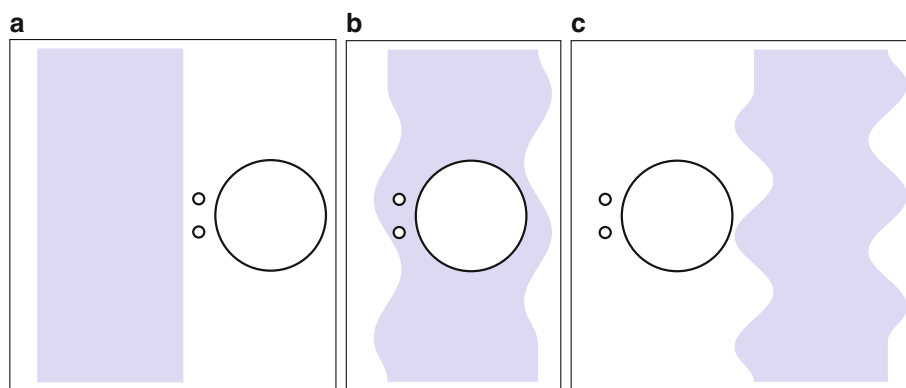


Fig. 9 Illustration of an antennule at various stages of a downstroke as it passes through an odorant filament. The shaded region shows the area that constitutes the odorant. The antennule starts **a** in front of the filament, **b** gets completely immersed in the filament and **c** traverses

through the odorant filament toward the end of the downstroke. This sequence is repeated in reverse order as the antennule comes back through the filament during the return stroke

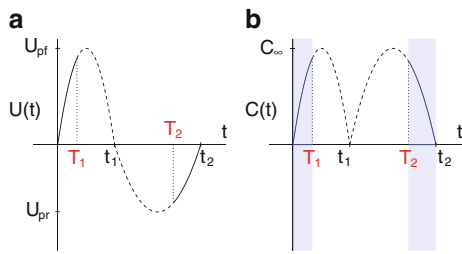


Fig. 10 Boundary conditions for **a** velocity and **b** odorant concentration for an odorant filament placed at the start of a downstroke. The *solid lines* and the *shaded region* show the portion of the flick that is spent by the antennule inside the filament. Odorant filaments grow thicker as both T_1 and T_2 move closer to t_1

(Fig. 11a) and end (Fig. 11b) of a flick, thinner filaments correspond to lower concentrations sampled.

Variations in mean odorant concentration transported to the surfaces of aesthetascs due to changes in antennule morphology and flicking kinematics are shown in Fig. 11. The gap width between adjacent aesthetascs was modified between 0.1 and 5 aesthetasc diameters (Fig. 11c). Molecule capture rises slightly with an increase in gap width and creates a significantly more uniform distribution of molecules around the aesthetasc surface. Increasing the antennule flicking speed enhances odorant molecule capture up to approximately twice the typical flick speed, above which odorant molecule capture declines for faster flick speeds (Fig. 11d). Figure 11e shows the change in mean concentration sampled along the length of the aesthetasc from the proximal end to distal tip. The data revealed a clear trend of increased mean concentration sampled from the proximal end to the basal tip of the aesthetasc. Since only the distal two-fifths of the aesthetasc sensillum is believed to be permeable to odorant molecules, this region is able to sample greater relative concentrations. In addition, we modeled the odorant transport assuming that aesthetascs were longer than their typical length of 100 μm . The sampled odorant concentration increases with longer aesthetascs, even up to twice their normal length. The flushing efficiency, quantified as the fraction of old molecules displaced by new molecules during subsequent flicks, was determined as a function of aesthetasc spacing, flick

speed, and position of sensing along the length of an aesthetasc (Fig. 12). This *flushing efficiency* signifies the effectiveness of a subsequent, second flick to replace previously captured odorants along the surface of the aesthetasc. Flushing efficiency increases with both aesthetasc spacing (Fig. 12a) and flick speed (Fig. 12b). In addition, increased flushing efficiency occurs at further distal distances along the length of the aesthetasc (Fig. 12c). For all cases, increases in aesthetasc spacing, flick speed and distal distance along the aesthetasc decrease the variability of odorant concentrations sampled at different locations along the circumference of the aesthetasc.

Although increases in aesthetasc spacing and length, as well as flick speed increases the ability for crayfish to sample new odors, these animals must also be able to discretely sample their fluid environment. Therefore, a balance of these two competing processes is necessary for *P. clarkii* to sample new odors during a downstroke flick but retain these odors over sufficient time periods during the return stroke. Figure 13 shows time courses of odorant concentration along the aesthetasc surface for different values of aesthetasc spacing. For aesthetasc spacing of $g/d \geq 1$, these plots indicate odorant capture at concentrations near ambient levels ($C/C_\infty > 0.9$) at the end of the downstroke, with sharp declines in odorant capture for $g/d < 1$. However, during the return stroke (time periods > 100 ms) larger gap spacings between aesthetascs show a greater loss of concentration, indicating a more ‘leaky’ return stroke that prevents discrete sampling of the same odorant laden fluid sample. A balance between greater sampling of new odorants during the downstroke, with retention of these odorants during the return stroke appears to occur with an aesthetasc spacing in the range of one hair diameter ($g/d = 1$).

Figure 14 shows time courses of odorant concentration at the aesthetasc surface for different flick speeds. For faster flick speeds, these plots indicate odorant capture at concentrations near ambient levels ($C/C_\infty > 0.9$) at the end of the downstroke, with sharp declines in odorant capture for $v/v_o < 1$. However, during the return stroke, large variations in odorant concentration are evident for fast flick speeds, indicating a more ‘leaky’ return stroke that

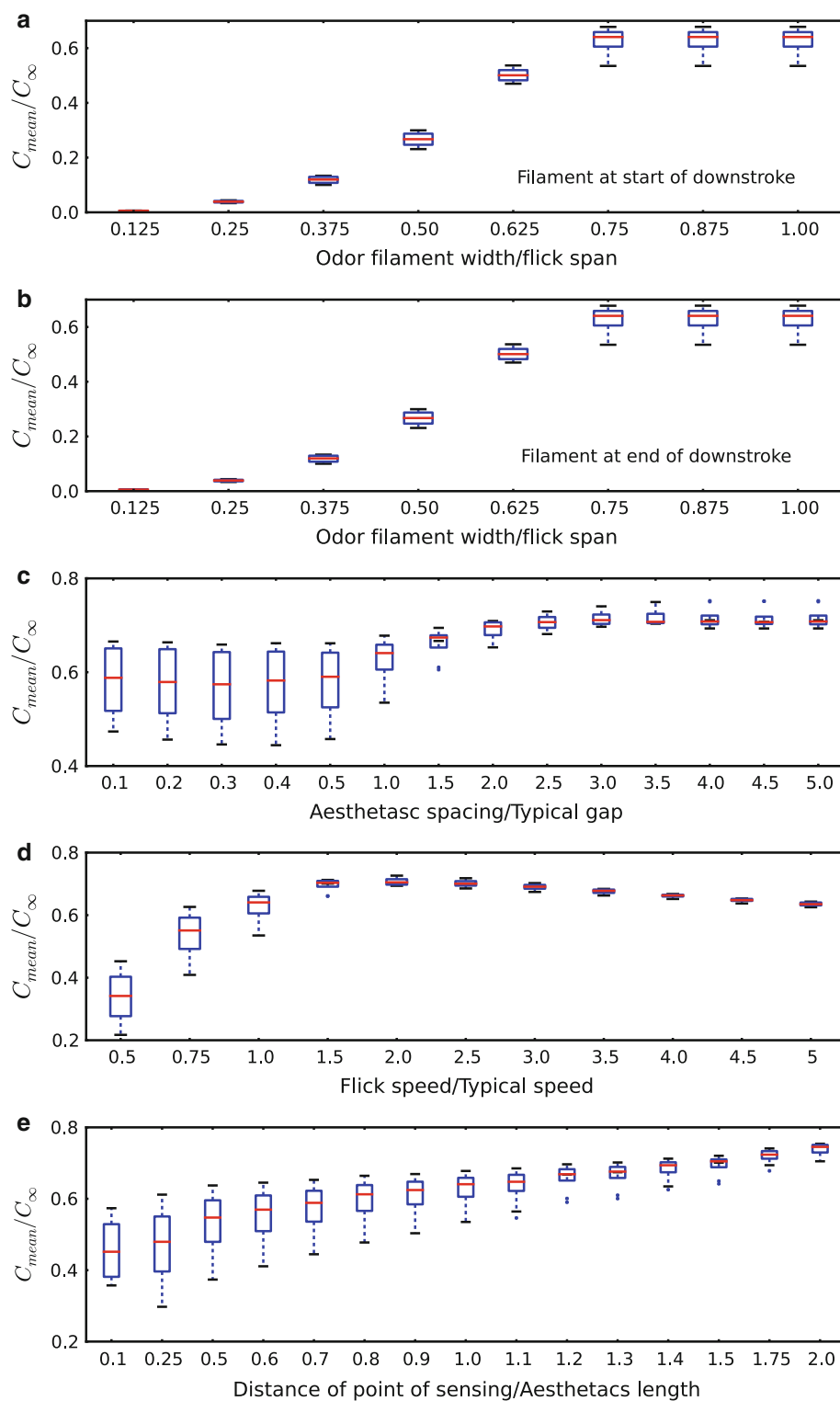
Table 1 Values of T_1 and T_2 (the time instants that signify the temporal bounds of an odorant filament as shown in Fig. 10) for filaments encountered at the *beginning* of a flick

T_1 (s)	$0.125 t_1$	$0.25 t_1$	$0.375 t_1$	$0.5 t_1$	$0.625 t_1$	$0.75 t_1$	$0.875 t_1$
T_2 (s)	0.2752	0.2536	0.2320	0.2106	0.1896	0.1695	0.1518

Table 2 Values of T_1 and T_2 (the time instants that signify the temporal bounds of an odorant filament as shown in Fig. 10) for odorant filaments encountered at the *end* of a flick

T_1 (s)	$0.125 t_1$	$0.25 t_1$	$0.375 t_1$	$0.5 t_1$	$0.625 t_1$	$0.75 t_1$	$0.875 t_1$
T_2 (s)	0.2632	0.2455	0.2253	0.2044	0.1830	0.1614	0.1396

Fig. 11 Variation of normalized mean concentration of odorant molecules around the aesthetasc surface with **a** odorant filaments of various width encountered during the beginning of the downstroke motion of a flick, **b** odor filaments of various width encountered during the end of the downstroke, **c** aesthetasc spacing, **d** flick speed, and **e** position of sensing at different distal distances along the length of an aesthetasc. *Boxplots* indicate the variation of odorant concentration transported to the surface of the aesthetasc (Fig. 6 shows the time courses for concentration at four different points around the aesthetasc surface). *Horizontal line* within the *box* indicates the median, while the lower and upper edges of the *box* represent the 25th and 75th percentiles, respectively. *Vertical lines* extending from the *box* indicate the minimum and maximum measured values



prevents discrete sampling of the same odorant laden fluid sample. Similar to *g/d* spacing, a balance between greater sampling of new odorants during the downstroke, with retention of these odorants during the return stroke, appears to occur at speeds similar to that at which *P. clarkii* have been observed to flick (i.e., $v/v_o = 1$).

Discussion

A numerical model of the antennule and aesthetasc structure of the freshwater crayfish, *P. clarkii*, was developed to simulate the advective–diffusive transport of odorant molecules to aesthetasc surfaces. The first step in the

Fig. 12 Flushing efficiency, quantified as the fraction of old molecules displaced by new molecules during subsequent flicks, plotted in relation to **a** aesthetasc spacing, **b** flick speed, and **c** position of sensing at different distal distances along the length of an aesthetasc. *Boxplots* are described in Fig. 11. Smaller *boxplots* indicate more uniform concentrations sampled along the circumference of the aesthetasc

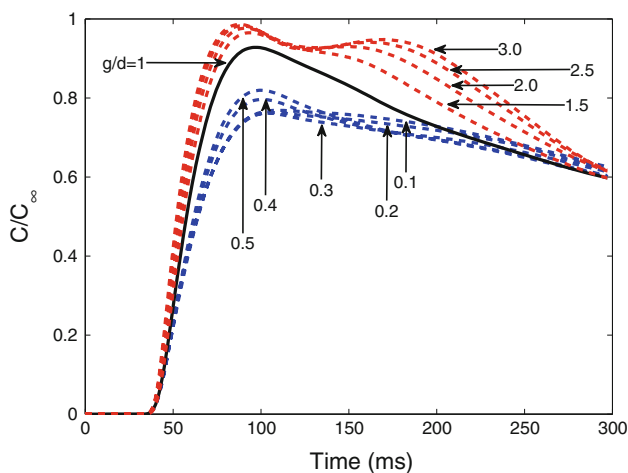
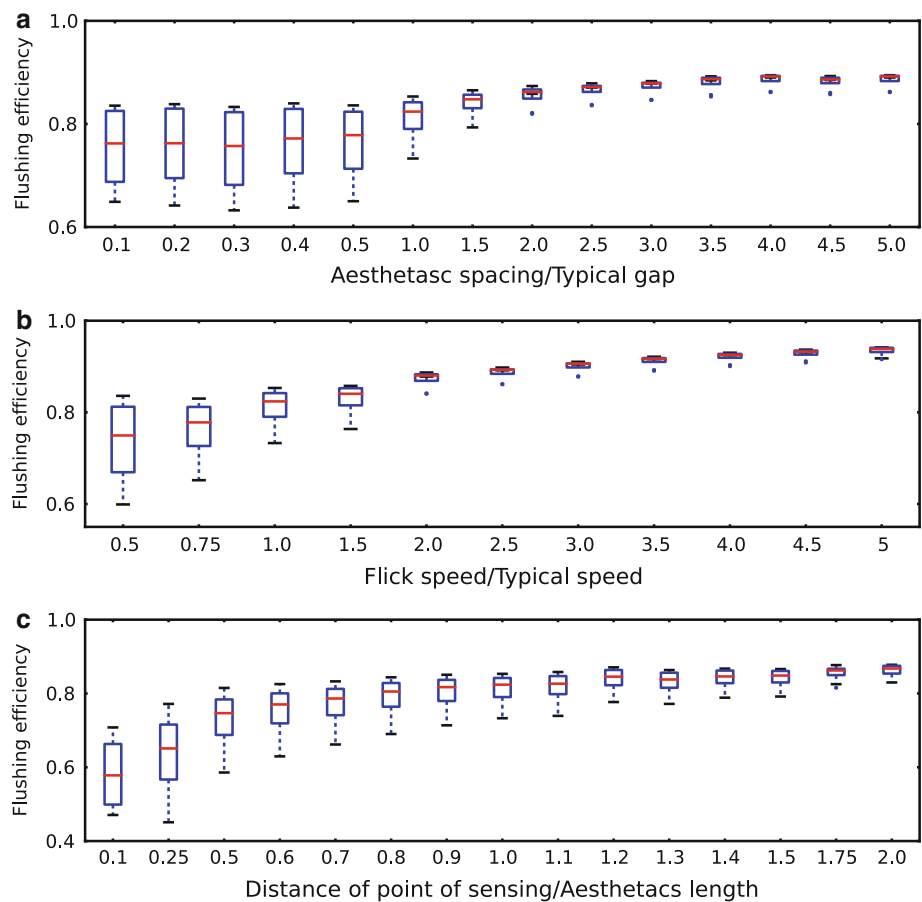


Fig. 13 Variation of normalized odorant concentration with time during a flick-return sequence for different values of g/d at $v = v_0$. g/d ratios for each line are labeled in the figure

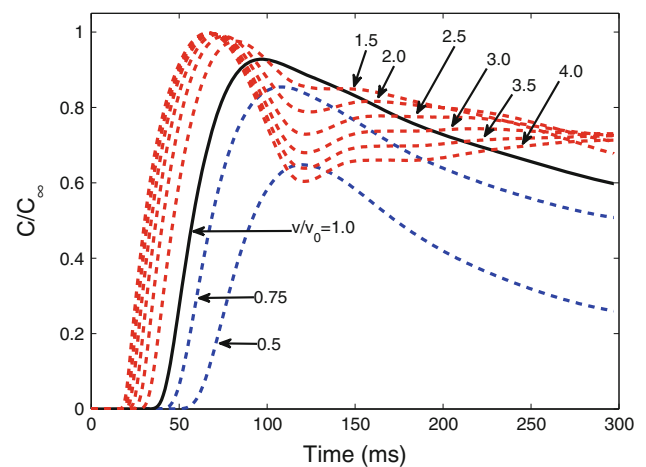


Fig. 14 Variation of normalized odorant concentration with time during a flick-return sequence for different flick speeds at $g/d = 1$. v/v_0 ratios for each line are labeled in the figure

process of sniffing is the interception by an olfactory organ of odorants in the surrounding air or water. Our results show that the rapid downstroke of the antennules facilitates transport of odorant molecules to the region surrounding the aesthetascs, while the slower return stroke enables for

additional time for the entrapped odorants to molecularly diffuse to the aesthetasc surfaces. The quantity of odorant molecules present at the aesthetasc surface reaches peak values near the end of downstroke, but due to the comparatively slow nature of the return stroke, significant

concentrations of odorant are retained in the vicinity of the aesthetascs at the end of the flick/return sequence. Subsequent flicks were shown to remove the odorants captured during the previous flick and capture new odorants from the ambient flow, at a replacement rate of up to 97.6 %. Thus, flicking provides a mechanism to discretely sample the odorant-laden fluid environment in both space and time while the animal navigates within a plume.

Although early models of odorant tracking assumed that animals respond to time-averaged concentration gradients in a plume (Bossert and Wilson 1963), the rapidity of plume tracking maneuvers by crustaceans and insects suggests that discrete sampling of time-varying odorant concentrations is necessary to locate an odorant source (Vickers 2006; Webster and Weissburg 2009). The plume tracking success of crustaceans (Weissburg and Zimmerfaust 1993; Jackson et al. 2007) and insects (Vickers 2006) has been found to be lower in homogeneous plumes than in intermittent plumes. Likewise, the frequency of odorant encounters by crayfish affects their walking speed while searching for the source (Mead et al. 2003; Page et al. 2011). This suggests that successful plume tracking depends on discrete sampling of the filamentous structure of an odorant plume (Atema 1996; Derby et al. 2001; Webster and Weissburg 2009) and flicking provides a mechanism to achieve this.

Overall, for crayfish it is not known how long odorant molecules need to be in contact with chemosensory cells, or in what concentration to initiate a response. After reaching the surface of a sensillum, odorant molecules must still diffuse through the cuticle, through the extracellular space, and to receptors on the dendrites of ORN. The patterns of action potentials that those neurons produce in response to odorants, and processing of those signals in the brain, ultimately determine whether or not the odorants are detected by the animal (Ache and Young 2005; Wilson 2008; Su et al. 2009). For the spiny lobster, *Panulirus argus*, or a clawed lobster, *Homarus americanus*, when an odorant pulse is delivered to the aesthetascs, receptor neurons in the antennule respond (after a latency period of ~70–500 ms) with a series of action potentials (spikes) that last ~100–200 ms, followed by a period of decline in the frequency and amplitude of spikes (Gomez and Atema 1996b; Marschall and Ache 1989). Both the maximum spike frequency and the total number of spikes correlate with the onset slope and amplitude of concentration change above background (Gomez and Atema 1996b; Zettler and Atema 1999; Marschall and Ache 1989; Derby et al. 2001). For the crayfish numerical model, peak concentrations at the aesthetasc surface were found to occur at approximately 50 ms after the initiation of the flick and odorant molecules remain in contact with the aesthetasc surface until the initiation of the subsequent flick.

The duration over which animals are exposed to odorants is also important in neural coding. For example, the antennal receptor neurons in *H. americanus* require at least 50 ms of odorant stimulus to fire, but ≥ 200 ms for the spike frequency to reflect the concentration increase of the odorant pulse (Gomez and Atema 1996b). However, if an odorant stimulus lasts too long, chemoreceptor cells undergo adaptation, i.e. their response to another odorant pulse of the same or lower concentration is reduced or absent. Lobster antennule receptor neurons start to adapt after continuous exposure to an odorant stimulus of 300 ms, and are completely adapted after 1000 ms exposure (Gomez et al. 1999). Such adaptation resets the sensitivity of the neuron such that it can respond to pulses of odorant concentration higher than background, thereby remaining sensitive to transient increases in odorant concentration in environments where the background concentration varies (Borroni and Atema 1988). For the crayfish model, the aesthetascs were observed to encounter an odorant concentration of more than 90 % ambient concentration at the end of the downstroke flick, and retain greater than 60 % of the ambient concentration by the end of the return stroke, thus enabling the aesthetasc to be exposed to concentration over the duration of the flick (approximately 240 ms) and sufficient time for neurons to respond to the presence of odorants. Subsequent flicks showed exchange of these odorants with either new odorants or no-odor for the case of flicking into odorant-free water, which may prevent *P. clarkii* neurons from undergoing adaptation to continual exposure to odorants on timescales of 300 ms and greater.

The frequency of repeated odorant pulses can also affect neural responses. If an odorant stimulus starts ≥ 400 ms after the previous one ends, antennule olfactory receptor cells of *H. americanus* can resolve them as separate pulses, but if it arrives ≤ 200 ms after the previous odorant has stopped, then the neuron responds as though the second pulse is a continuation of the previous one (Gomez and Atema 1996a). The bursts of firing by antennule ORN of *P. argus* adapt selectively to odorant pulses at frequencies of 0.5–0.1 Hz (Marschall and Ache 1989). The flicking rate of the crayfish was measured to be $3.3 \text{ flicks s}^{-1}$, which falls within the minimum range that aquatic organisms need to be exposed to odorants of 50 ms, but less than the time at which adaptation to odorants begins to occur of 300 ms (Gomez and Atema 1996b). Taken together, intermittency in odorant sampling is important to both initiate receptor neuron responses to odorants and to limit adaptation to these odorants.

Aesthetasc spacing and length

Both the antennule morphology and the flicking kinematics of *P. clarkii* were altered through changes in the numerical

model to determine their impacts on odorant transport to aesthetasc surfaces. The variation of the spacing between adjacent aesthetascs has a noticeable effect on variations in concentration levels in the region between the aesthetascs, as well as the flux of odorants to their surfaces. The aesthetascs are typically spaced one aesthetasc diameter apart. An aesthetasc gap width greater than one diameter allows larger quantities of odorant molecules to pass between them during the downstroke, but also increases the ‘leakiness’ of these trapped odorants during the return stroke (Cheer and Koehl 1987). Leakiness becomes important with regard to how morphology and velocity impact delivery of odorants to sensory cells. When leakiness is large, boundary layers are reduced as water is allowed to pass through adjacent hairs. This enhanced odorant transport decreases the distance across which diffusion must occur to reach sensory cells. However, for antennules exposed to high ambient currents, such a system would not allow for discrete sampling of odorants during a flick. Interestingly, no matter how wide the gap, odorant concentrations at the aesthetasc surface never reach 100 % ambient concentration during the flick/return sequence, suggesting that although the thickness of the diffusive boundary layer is reduced during the flick, it is not removed entirely.

Various locations along the length of the aesthetasc, ranging from points near the base to well beyond the average aesthetasc length for a hypothetically longer aesthetasc, were tested to determine the effect of location on the aesthetasc on odorant detection. Results revealed that larger amounts of molecules were entrapped toward the distal two-thirds of the aesthetasc, where there is a transparent cuticle that is thought to allow rapid transport of odorants to chemosensory cells (Mellon 2005), than along the proximal end close to the attachment point along the antennule. In addition, enhanced odorant capture occurs with longer aesthetascs beyond the typical aesthetasc length, suggesting rapid breakdown of boundary layers near the tip, which facilitates greater exposure of the aesthetasc surface to incoming odorants. However, again, this enhances ‘leakiness’ of the flow between aesthetascs during the return stroke, limiting the ability of the olfactory organ to take discrete samples of odorant-laden fluid.

Flick speed

The number of odorant molecules encountered by the aesthetasc per unit of its surface area increases with Re of the flick, even though the aesthetasc experiences the odorant flux for a longer duration for slower flick speeds. The flick speed, and hence the Reynolds number, both have direct impact on the flow of odorants through the aesthetasc arrays and how rapidly the odorant molecules contact the aesthetasc surface. At high flick speeds, where rates are greater than double

typical speeds, odorant concentrations along the aesthetasc surface increase quickly, and near the end of the downstroke, a pronounced flow reversal occurs, causing a large proportion of the odorant molecules present between the aesthetascs to get washed away during the return stroke. However, for slower speeds, this flow reversal does not appreciably occur and odorants are more effectively ‘trapped’ within the aesthetasc hair array throughout the flick sequence.

Although a wide diversity of antennule morphologies and flick speeds occur across many species that allow animals to take discrete samples of their fluid environment (Koehl 2006, 2011), our findings indicate that *P. clarkii* flicks its antennules at speeds which maximizes the difference in fluid leakiness between the downstroke and return stroke. In addition, our results extend this idea to show (in Figs. 13, 14) that this discrete fluid sampling maximizes odorant delivery to aesthetasc surfaces during the flick/return sequence.

Odorant filament width

Changes in odorant filament width and their impact on transport of odorants suggest that very low concentrations, relative to ambient levels, are encountered along aesthetasc surfaces for thin odorant filaments. For odorant filaments of thickness 1 mm or less (i.e., less than 50 % of the flick distance of 2 mm), concentrations of $C \leq 0.5C_\infty$ were encountered along the aesthetasc surface, regardless of whether odorant filaments were positioned at the start or the end of the downstroke. For wider filaments, high concentrations are encountered and asymptote to peak concentration levels for filaments with a 2 mm thickness; close to the distance over which a flick spans. At these 1–2 mm filament thicknesses, filaments encountered at the beginning of a flick capture more molecules than filaments encountered at the end of the downstroke.

Conclusions regarding antennule flicking and odorant detection by *P. clarkii*

Behavioral studies have indicated that the instantaneous spatial distribution of odorants sampled by olfactory organs at different locations within a plume can provide important cues for tracking (Webster and Weissburg 2009; Weissburg et al. 2002; Keller and Weissburg 2004). The intermittency in odorant encounters, the duration over which animals are exposed to odorants, and changes in the onset slope of concentrations along the aesthetasc surface all appear to be important parameters that impact the response of organisms to its odorant environment (Zettler and Atema 1999). Our results suggest that flicking (1) enhances the ability for crayfish to discretely sample their odor environment due to rapid replacement of odorants during successive flicks,

(2) offsets adaptation of chemosensory neurons that may occur due to continued exposure to odorants and (3) reduces the chance of flicker-fusion, where two different odorant filaments are perceived as one (Gomez et al. 1999). The spike response of the ORN neuronal targets within the brain to the changes in concentrations and odorant encounter rates have been documented for crayfish (Mellon and Humphrey 2007) and findings from our numerical model suggest that ORN responses are directly impacted by morphological parameters and flow scenarios that control the transport of odorant molecules to aesthetasc surfaces.

The receptor neurons located within aesthetascs respond to concentration gradients in a turbulent plume by producing a series of action potential spikes. The spike pattern that these neurons produce in response to odorants, along with processing of these signals in the brain, determines whether odorants are detected by the animal (Wilson 2008; Su et al. 2009). The spike frequency is higher for steeper concentration gradients, but spike counts revert to zero or low levels during exposure to persistently high odorant concentrations (Zettler and Atema 1999), suggesting swift adaptation of chemoreceptor cells to background concentration levels. As found in this study, increasing the gap spacing between aesthetascs, increasing the flick speed, and increasing aesthetasc length each creates (1) quicker attainment of peak concentrations, (2) higher concentrations surrounding the aesthetascs and (3) a more uniform distribution of odorants around the aesthetasc surface. These changes to antennule morphology and kinematics increase exposure to ambient odorants, but may also provide poor conditions for discrete sampling of the odor environment or cause adaptation of chemoreceptor cells. Our results also suggest that through changes in both the timing and the encounter rate of odorant molecules to aesthetasc surfaces caused by antennule flicking, odorant filaments of varying thickness and concentration can be distinguished, which has been shown to vary in systematic ways with distance from the source (Reidenbach and Koehl 2011; Weissburg et al. 2002). Therefore, for *P. clarkii* both the sampling behavior and the neural responses to odorants involved in olfaction appear well suited to the intermittent spatial and temporal distribution of odorants within the environment.

Acknowledgments This research was supported by a National Science Foundation grant NSF-CBET-0933034. We thank two anonymous reviewers for their helpful comments that improved the manuscript.

References

- Ache BW, Young JM (2005) Olfaction: diverse species, conserved principles. *Neuron* 48:417–430
- Adam G, Delbrück M (1968) Structural chemistry and molecular biology. Freeman, San Francisco, pp 198–215
- Atema J (1995) Chemical signals in the marine environment: dispersal, detection, and temporal signal analysis. *Proc Natl Acad Sci USA* 92(1):62–66
- Atema J (1996) Eddy chemotaxis and odor landscapes: exploration of nature with animal sensors. *Biol Bull* 191:129–138
- Beltz BS, Kordas K, Lee MM, Long JL, Benton JB, Sandeman DC (2003) Ecological, evolutionary and functional correlates of sensilla number and glomerular density in the olfactory system of decapod crustaceans. *J Comp Neurol* 455:260–269
- Berg HC, Purcell EM (1977) Physics of chemoreception. *Biophys J* 20(2):193–219
- Boeckh J, Kaissling K, Schneider D (1965) Insect olfactory receptors. *Cold Spring Harb Symp Quant Biol* 30:263–280
- Borroni PF, Atema J (1988) Adaptation in chemoreceptor cells. *J Comp Physiol A* 164:67–74
- Bossert WH, Wilson EO (1963) The analysis of olfactory communication among animals. *J Theor Biol* 5:443–469
- Cheer A, Koehl M (1987) Fluid flow through filtering appendages of insects. *Math Med Biol* 4(3):185
- Crimaldi JP, Koseff JR (2001) High-resolution measurements of the spatial and temporal scalar structure of a turbulent plume. *Exp Fluids* 31(1):90–102
- Denny MW (1993) Air and water. Princeton University Press, Princeton
- Derby CD, Steullet P, Horner AJ, Cate HS (2001) The sensory basis of feeding behaviour in the Caribbean spiny lobster, *Panulirus argus*. *Mar Freshwater Res* 52:1339–1350
- DeSimone JA (1981) Physicochemical principles in taste and olfaction. In: Cagan RH, Kane MR (eds) *Biochemistry of taste and olfaction*. Academic Press, New York, pp 213–229
- Futrelle R (1984) How molecules get to their detectors: the physics of diffusion of insect pheromones. *Trends Neurosci* 7(4):116–120
- Getchell TV, Getchell ML (1977) Early events in vertebrate olfaction. *Chem Senses* 2(3):313
- Gomez G, Atema J (1996a) Temporal resolution in olfaction II: time course of recovery from adaptation in lobster chemoreceptor cells. *J Neurophysiol* 76:1340–1343
- Gomez G, Atema J (1996b) Temporal resolution in olfaction: stimulus integration time of lobster chemoreceptor cells. *J Exp Biol* 199:1771–1779
- Gomez G, Voigt R, Atema J (1999) Temporal resolution in olfaction III: flicker fusion and concentration-dependent synchronization with stimulus pulse trains of antennular chemoreceptor cells in the American lobster. *J Comp Physiol A* 185:427–436
- Grasso FW, Basil JA (2002) How lobsters, crayfishes, and crabs locate sources of odor: current perspectives and future directions. *Curr Opin Neurobiol* 12(6):721–727
- Horner AJ, Schmidt M, Edwards DH, Derby CD (2008) Role of the olfactory pathway in agonistic behavior of crayfish, *Procambarus clarkii*. *Invertebr Neurosci* 8(1):11–18
- Humphrey J, Mellon D (2007) Analytical and numerical investigation of the flow past the lateral antennular flagellum of the crayfish *Procambarus clarkii*. *J Exp Biol* 210(Pt 17):2969
- Jackson JL, Webster DR, Rahman S, Weissburg MJ (2007) Bed-roughness effects on boundary-layer turbulence and consequences for odor-tracking behavior of blue crabs (*Callinectes sapidus*). *Limnol Oceanogr* 52:1883–1897
- Johnson ME, Atema J (2005) The olfactory pathway for individual recognition in the American lobster *Homarus americanus*. *J Exp Biol* 208:2865–2872
- Keller TA, Weissburg MJ (2004) Effects of odor flux and pulse rate on chemosensory tracking in turbulent odor plumes by the blue crab, *Callinectes sapidus*. *Biol Bull* 207:44–55
- Keller TA, Powell I, Weissburg MJ (2003) Role of olfactory appendages in chemically mediated orientation of blue crabs. *Mar Ecol Prog Ser* 261:217–231

- Koehl MAR (2006) The fluid mechanics of arthropod sniffing in turbulent odor plumes. *Chem Senses* 31(2):93–105
- Koehl MAR (2011) Hydrodynamics of sniffing by crustaceans. In: Breithaupt T, Theil M (eds) *Chemical communication in crustaceans*. Springer, Berlin, pp 85–102
- Koehl MAR, Koseff JR, Crimaldi JP, McCay MG, Cooper T, Wiley MB, Moore PA (2001) Lobster sniffing: antennule design and hydrodynamic filtering of information in an odor plume. *Science* 294:1948–1951
- Lide DR (1991) *Handbook of chemistry and physics*. CRC Press, Boca Raton
- Mankin R, Mayer M (1984) The insect antenna is not a molecular sieve. *Cell Mol Life Sci* 40(11):1251–1252
- Marschall HP, Ache BW (1989) Response dynamics of lobster olfactory neurons during simulated natural sampling. *Chem Senses* 14:725
- Mead KS, Wiley MB, Koehl MAR, Koseff JR (2003) Fine-scale patterns of odor encounter by the antennules of mantis shrimp tracking turbulent plumes in wave-affected and unidirectional flow. *J Exp Biol* 206:181–193
- Mellon D (1997) Physiological characterization of antennular flicking reflexes in the crayfish. *J Comp Physiol A* 180(5):553–565
- Mellon D (2005) Integration of hydrodynamic and odorant inputs by local interneurons of the crayfish deutocerebrum. *J Exp Biol* 208:3711–3720
- Mellon D, Humphrey J (2007) Directional asymmetry in responses of local interneurons in the crayfish deutocerebrum to hydrodynamic stimulation of the lateral antennular flagellum. *J Exp Biol* 210:2961–2968
- Mellon D, Tuten HR, Redick J (1989) Distribution of radioactive leucine following uptake by olfactory sensory neurons in normal and heteromorphic crayfish antennules. *J Comp Neurol* 280(4):645–662
- Moore P, Crimaldi J (2004) Odor landscapes and animal behavior: tracking odor plumes in different physical worlds. *J Marine Syst* 49(1–4):55–64
- Moore P, Grills JL (1999) Chemical orientation to food by the crayfish *Orconectes rusticus*: influence of hydrodynamics. *Animal Behav* 58:953–963
- Moore P, Gerhardt GA, Atema J (1989) High resolution spatio-temporal analysis of aquatic chemical signals using microelectrochemical electrodes. *Chem Senses* 14(6):829
- Murray JD (1977) *Nonlinear-differential-equation models in biology*. Oxford University Press, Oxford
- Nachbar RB, Morton TH (1981) A Gas chromatographic (GLPC) model for the sense of smell. Variation of olfactory sensitivity with conditions of stimulation. *J Theor Biol* 89(3):387–407
- Page JL, Dickman BD, Webster DR, Weissburg MJ (2011) Getting ahead: context-dependent responses to odorant filaments drive along-stream progress during odor tracking in blue crabs. *J Exp Biol* 214:1498–1512
- Reidenbach MA, Koehl M (2011) The spatial and temporal patterns of odors sampled by lobsters and crabs in a turbulent plume. *J Exp Biol* 214(18):3138–3153
- Reidenbach MA, George N, Koehl M (2008) Antennule morphology and flicking kinematics facilitate odor sampling by the spiny lobster, *Panulirus argus*. *J Exp Biol* 211(17):2849
- Schmitt BC, Ache BW (1979) Olfaction: responses of a decapod crustacean are enhanced by flicking. *Science* 205:204–206
- Schuech R, Stacey MT, Barad MF, Koehl MAR (2012) Numerical simulations of odorant detection by biologically inspired sensor arrays. *Bioinspir Biomim* 7(1):16001
- Stacey MT, Mead KS, Koehl MAR (2002) Molecule capture by olfactory antennules: mantis shrimp. *J Math Biol* 44(1):1–30
- Su CY, Menzies K, Carlson JR (2009) Olfactory perception: receptors, cells and circuits. *Cell* 139:45–59
- Vickers NJ (2006) Winging it: moth flight behavior and responses of olfactory neurons are shaped by pheromone plume dynamics. *Chem Senses* 31:155–166
- Webster DR, Weissburg MJ (2001) Chemosensory guidance cues in a turbulent chemical odor plume. *Limnol Oceanogr* 46:1034–1047
- Webster DR, Weissburg MJ (2009) The hydrodynamics of chemical cues among aquatic organisms. *Annu Rev Fluid Mech* 41:73–90
- Weissburg MJ, Zimmer-Faust RK (1993) Life and death in moving fluids: hydrodynamic effects on chemosensory-mediated predation. *Ecology* 74:1428–1443
- Weissburg MJ, Ferner MC, Pisut DP, Smee DL (2002) Ecological consequences of chemically mediated prey perception. *J Chem Ecol* 28:1953–1970
- Wilson RI (2008) Neural and behavioral mechanisms of olfactory perception. *Curr Opin Neurobiol* 18:408–412
- Zettler E, Atema J (1999) Chemoreceptor cells as concentration slope detectors: preliminary evidence from the lobster nose. *Biol Bull* 197:252–253